Bull. Mater. Sci., Vol. 32, No. 5, October 2009, pp. 493–498. © Indian Academy of Sciences.

Catalytic synthesis of ZnO nanorods on patterned silicon wafer—An optimum material for gas sensor

S K PANDA and C JACOB*

Materials Science Centre, Indian Institute of Technology, Kharagpur 721 302, India

MS received 22 September 2008; revised 21 November 2008

Abstract. **ZnO nanorods have been synthesized over etch-patterned Si (110) wafer using annealed silver thin film as growth catalyst. The growth of ZnO nanorods were performed by a two-step process. Initially, the deposition of Zn thin film was done on the annealed silver catalyst film over etch-patterned Si (110) substrate by thermal evaporation, and then annealed at 800°C in air. The etching of the patterned Si (110) wafers was carried out by 50% aqueous KOH solution. The samples were investigated by optical microscopy, scanning electron microscopy, X-ray diffraction, Raman spectroscopy and room temperature photoluminescence spectroscopy. 'V' shaped grooves with no undercut were formed after etching due to the anisotropic nature of the KOH etchant. The etch-patterned wafer was used to provide larger surface area for ZnO growth by forming 'V'-grooves. This ZnO film may be predicted as a very good material for gas sensor.**

Keywords. **Patterned wafer; anisotropic etching; nanorods; catalytic growth; surface enhanced Raman scattering; sensor material.**

1. Introduction

Semiconductor gas sensors have attracted great attention over the last few decades due to their remarkable properties such as high sensitivity, low cost, easy fabrication and compatibility with silicon substrates. Semiconducting oxides, like Ga_2O_3, ZnO, SnO_2, TiO_2, etc are known to be potential materials for gas sensor (Mitra *et al* 1998; Hoefer *et al* 2001; Ruiz *et al* 2003). Among them, ZnO was one of the earliest sensors developed and capable of detecting a wide variety of gases like H_2, NH_3, CO, C_2H_5OH, NO_2, etc (Rao 2000; Shishiyanu *et al* 2005; Rout *et al* 2006a; Sarala Devi *et al* 2006; Hsueh *et al* 2007). Recently, one-dimensional ZnO structures such as nanorods (Zhang *et al* 2005), nanowires (Hongsith *et al* 2008), nanobelts (Choopun *et al* 2007), nanotetrapods and nanomultipods (Gao and Wang 2005) have replaced ZnO bulk and thin film as sensor materials due to their high surface to volume ratio. In addition to gas sensing, ZnO nanostructures are also very good candidates for application in optoelectronic devices such as blue, violet and ultraviolet (UV) light emitting diodes (LEDs) (Zhang *et al* 2007) due to their direct and wide bandgap and large exciton binding energy (60 meV). One-dimensional ZnO nanostructures have proved to be valuable candidates for field emission devices (Li *et al* 2007a), too.

Generally, oxide thin film gas sensors work at relatively high temperatures (~350°C) which limit their applications particularly in mining environments. The presence of a few metal particles with ZnO nanostructures like Pt, Pd, Ag, etc act as activators for gas sensing at lower temperatures with enhanced sensitivity and short recovery and response time (Xu *et al* 2000; Rout *et al* 2006b; Wang *et al* 2007).

A variety of techniques have been used for the deposition of high quality ZnO nanostructures such as metallorganic CVD (MOCVD) (Park *et al* 2006), vapour-phase transport (Reynolds *et al* 1996), sputtering (Kim *et al* 2000), sol–gel (Ahn *et al* 2007) and thermal evaporation (Panda *et al* 2008). Among them, thermal evaporation is relatively simple and cheap but applicable to low melting point, low decomposition or low sublimation point oxides only. A few noble metals and transition metals such as Au, Ag, Ni, Co and their nanoparticles influence growth (Li *et al* 2007b; Kirkham *et al* 2007) and structural/electronic properties of ZnO nanostructures. In this paper, the catalytic growth of ZnO nanostructures on etch-patterned Si (110) wafer for the development of sensor material for reducing gases has been discussed.

2. Experimental

Patterned silicon (110) wafers with an oxide mask (SiO_2) of 0·5 μm thickness were etched in an aqueous 50% KOH solution at 70°C for 10 min. A thin film of silver (thickness, ~1·4 μm) was deposited on the etch-patterned Si (110) substrates by thermal evaporation of metallic silver (purity, ~99·99%) without intentional heating of the

*Author for correspondence (cxj14_holiday@yahoo.com)

substrates. Before deposition, the etched wafers were cleaned with acetone in an ultrasonic bath followed by 5% HF etching for a few seconds to remove the native oxide from the exposed Si surface. The samples were then rinsed with DI water and dried in flowing dry nitrogen. The as-deposited silver films were annealed at 200°C for various time durations in air to form a silver island structure. ZnO nanorods were synthesized on the annealed silver template over etch-patterned wafer by a two-step process. At first, the deposition of Zn thin film was done on the annealed silver template by thermal evaporation, then annealing of the as-grown Zn film was subsequently performed at 800°C in air. All the depositions were done in a HIND HI VAC Model No. 12 A4D Vacuum Coating Unit with $\sim 10^{-5}$ torr chamber pressure. During deposition, the substrates were kept 15 mm above the source. The etch-patterned samples and the as-grown ZnO sample were then investigated by optical microscopy (Leica-DMRX), scanning electron microscopy (SEM) (JEOL-JSM 5800), energy dispersive X-ray spectroscopy (EDX) attached to SEM, X-ray diffraction (XRD) (Philips-PW-1710) and atomic force microscopy (AFM) (Nanonics SPM-100). Raman experiments were performed using a Laser Raman Microspectrometer (Renishaw RM 1000B) coupled with a Leica DMLM microscope. Room temperature photoluminescence spectroscopy was carried out using a pulsed Xenon discharge lamp (power equivalent to 20 kW for 8 μs duration) of 320 nm as the excitation source in a Perkin-Elmer LS-55 system.

3. Results and discussion

Figures 1a and b show the SEM images of the patterned silicon wafer before and after etching, respectively. V-grooves with no undercut (shown in figures 1c and d) were formed due to the anisotropic nature of the KOH etchant. KOH is an alkali hydroxide, generally used in anisotropic wet-etching of silicon and the etch rate of Si is maximum for the {110} planes and minimum for the {111} planes. KOH does not attack oxide mask signifi-

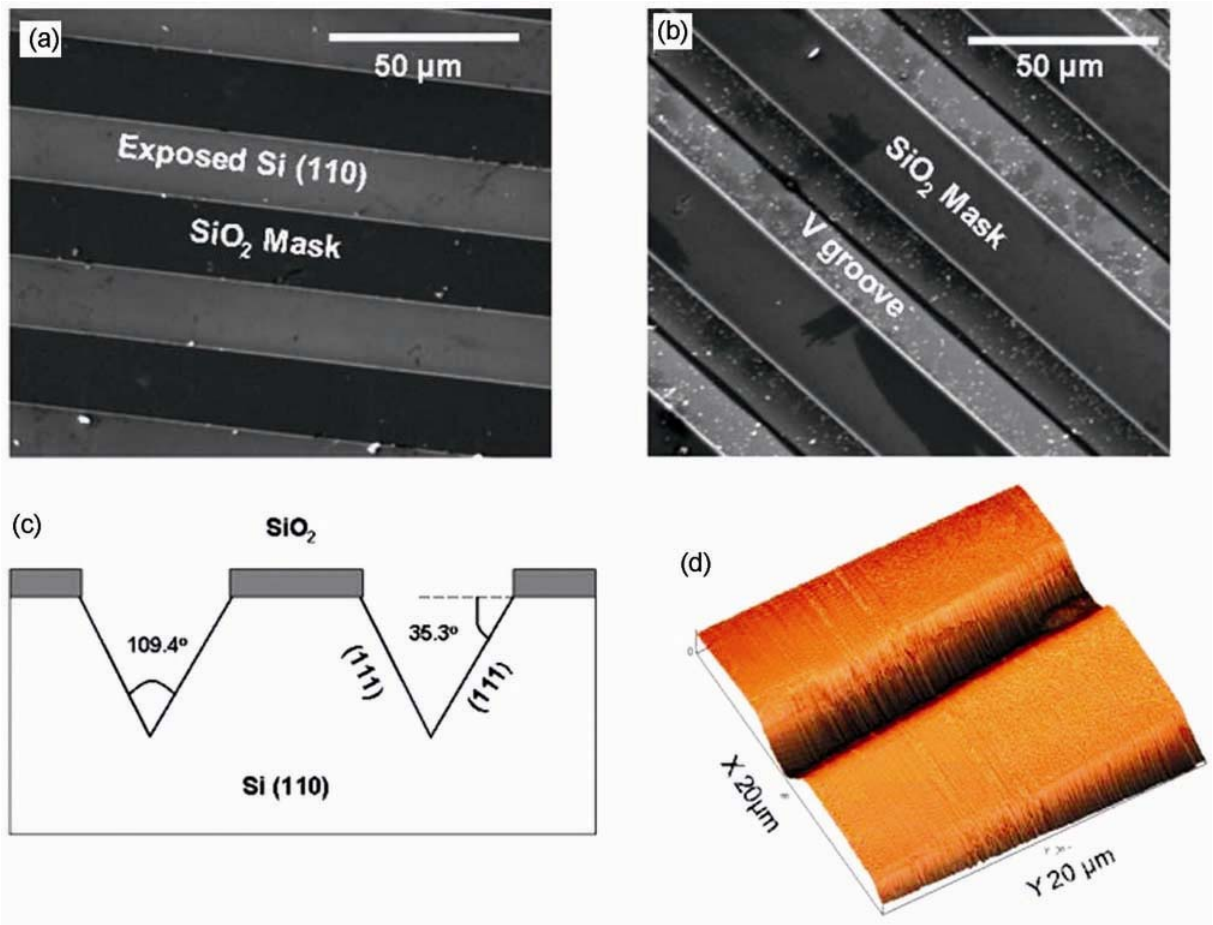

Figure 1. SEM micrographs of the patterned Si (110) wafer (**a**) before etching, (**b**) after 10 min etching using 50% aqueous KOH solution at 70°C, (**c**) schematic diagram of the etch-patterned Si (110) wafer and (**d**) AFM image of the 'V-groove'.

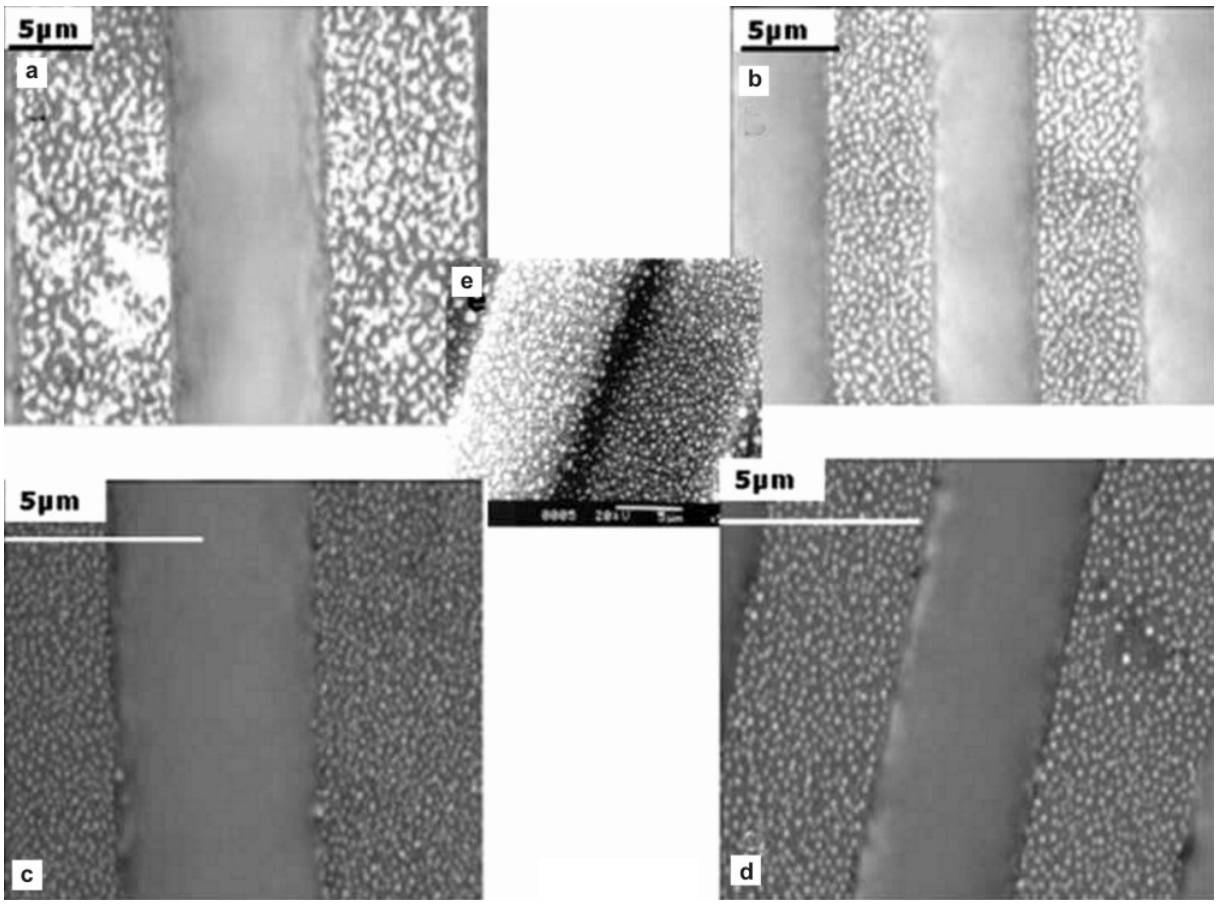

Figure 2. Optical micrograph of silver thin films after annealing at 200°C in air for various time durations: **a**. 15 min, **b**. 30 min, **c**. 45 min, **d**. 120 min and **e**. SEM image of silver island structures after 60 min annealing.

cantly at 70°C. Therefore, the exposed Si (110) region of patterned sample will be etched and etching will be stopped after some time when all the (111) planes are exposed. The schematic diagram of the etch-patterned sample is shown in figure 1c. The angle between (110) and (111) planes of silicon is 35·3° which leads to the formation of 'V'-shaped grooves.

Figure 2 shows the morphological change of the silver thin films on the etch-patterned Si wafers with annealing time. The SEM image of figure 2e indicates that the silver island structures were formed on both the oxide mask and in the 'V'-groove. The size and the number density of the silver islands decrease with increase in annealing time. A finer distribution of lightly populated silver islands was observed for 2 h annealed sample. This 2 h annealed silver film on etch-patterned Si wafer was used as the template for ZnO nanostructure growth.

Figure 3 shows the SEM images at different magnifications of ZnO nanorods on etch-patterned Si wafer by using annealed Ag as catalyst. Sword-like ZnO nanorods with sharp tips were found to grow on both the oxide mask and in the 'V'-groove of the patterned wafer. The nanorods are densely populated and arbitrarily directed and most of them are non-coplanar with the substrate surface.

In the present study, the annealed silver thin film was used as catalyst for the nanorod growth and the growth mechanism of the ZnO nanorods is different from the conventional VLS mechanism. At the annealing temperature of the Zn film (800°C), Zn remains in the liquid phase (melting point of Zn is 419°C) and as the radius of Zn atoms is smaller than the radius of silver atoms, Zn begins to diffuse into the silver matrix. At 800°C, the maximum solid solubility of Zn in silver is around 12 wt% and beyond 15 wt% of Zn concentration and a homogeneous Ag/Zn liquid alloy forms near the interface (Massalski 1990). This liquid alloy becomes saturated by Zn with increase in annealing time and results in the precipitation of Zn particles. The precipitated Zn particles recombine with oxygen and oxidize to form many ZnO nuclei on the surface of the Ag–Zn alloy. These ZnO nuclei begin to grow one-dimensionally with further increase in annealing time to form sword-like ZnO nanorods. Here, annealing of the Ag films is the key factor for dense nanostructure growth (Li *et al* 2007a). To study the

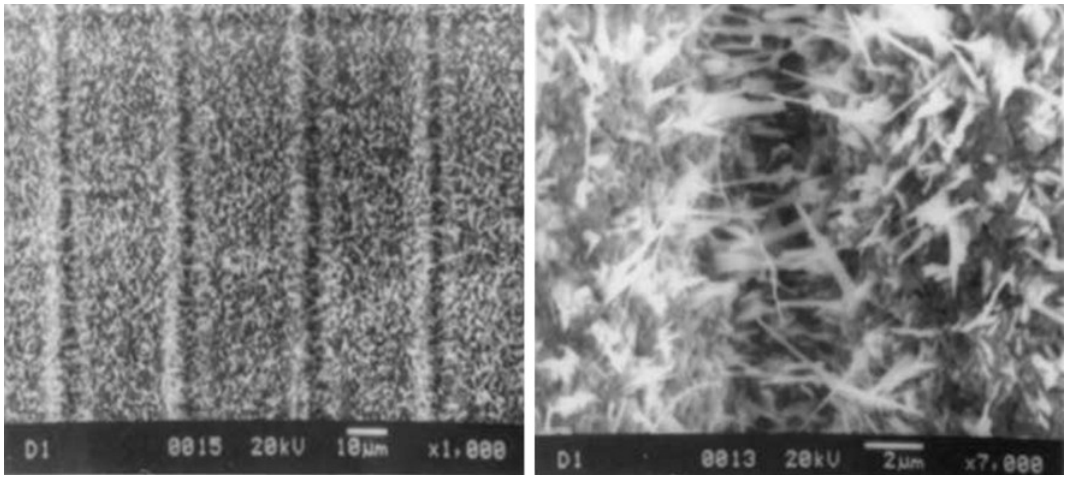

Figure 3. SEM images of the ZnO nanostructures at different magnifications grown on annealed Ag template over etch-patterned Si wafer.

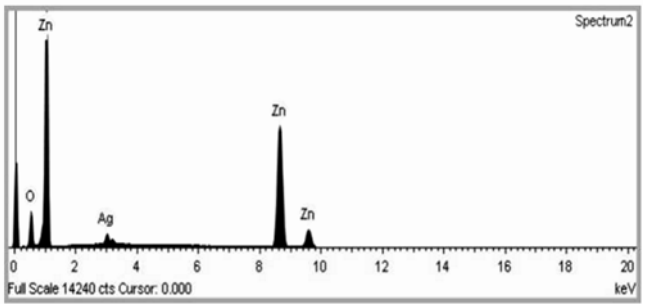

Figure 4. Energy dispersive X-ray spectroscopy (EDS) spectrum of the ZnO nanorods.

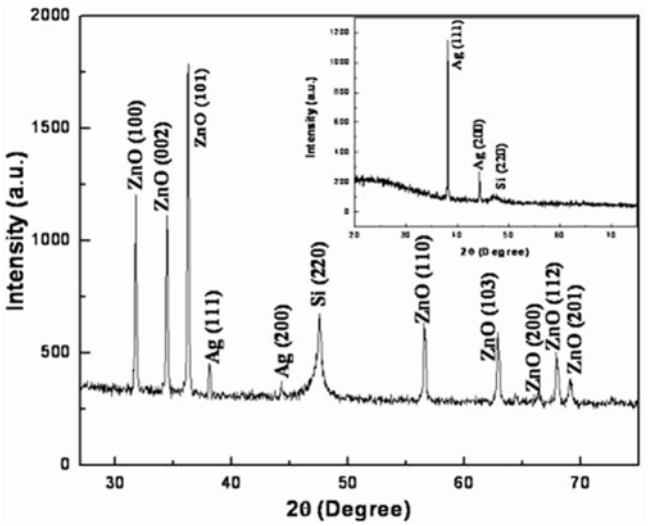

Figure 5. XRD θ–2θ scan of the ZnO nanorods using Cu Kα (λ = 1·54056 Å) line. Inset shows the XRD pattern of annealed Ag film.

role of silver on nanostructure growth, Zn thin film was deposited directly on Si (111) substrate and annealed under the same conditions as earlier. Instead of sword-like nanorods, needle-like ZnO nanorods with rounded tips were found to grow throughout the surface of the Si wafer. The details of the growth mechanism and characteristics of the needle-like nanorods have been discussed in our previous work (Panda *et al* 2009).

The energy dispersive X-ray spectroscopy (EDS) study of the ZnO samples focused on ZnO nanorods inside the groove is shown in figure 4. The bulk EDX spectrum shows that besides Zn and O, the sample contains a small amount of silver which comes from the catalyst particles.

The XRD pattern in figure 5 provides the microstructural information of the nanostructures grown on annealed Ag coated Si substrate. All the diffraction peaks in the diffraction pattern can be indexed to the known hexagonal wurtzite structure of ZnO with lattice parameter of $a = b = 3{\cdot}25$ Å and $c = 5{\cdot}207$ Å (JCPDS card no. 79-2205). The intense peak at 47·5° corresponds to Si (220) diffraction from patterned substrate and the peaks at 38·1° and 44·2° represents the Ag (111) and Ag (200), respectively (inset of figure 5), which are due to the catalyst particles.

The Raman spectra for the ZnO samples using 514·5 nm excitation wavelength is shown in figure 6. The measured Raman spectrum was compared with the frequency and symmetry of the fundamental Raman active phonon modes for ZnO crystal reported previously (Damen *et al* 1966) and it can be concluded that the peak at 436 cm^{-1} corresponds to E_2 (high), 374 cm^{-1} corresponds to A_1 (TO) and 565 cm^{-1} corresponds to A_1 (LO) and E_1 (LO) modes. The peak at ~331 cm^{-1} and a broad asymmetrical peak located between 1050 cm^{-1} and 1180 cm^{-1} are due to multi-phonon scattering process. The E_2 mode at 436 cm^{-1} has the highest intensity and narrow line width compared to other modes, which indicates that the nanorods are made of hexagonal wurtzite ZnO and

has good crystalline quality. In the Raman spectrum, the E_2 (high) peak at 436 cm^{-1} was shifted towards the lower Raman shift region by 3 cm^{-1} compared to bulk ZnO. The observed red shift of E_2 phonon peak may be due to the optical-phonon confinement by the nanocrystal boundaries or local laser heating (Alim *et al* 2005). The significant enhancement of Raman intensity of the A_1 (LO) and E_1 (LO) modes compared to the pure (purity > 99%) ZnO powder (inset of figure 6) produced by Merck Ltd, was observed which can be explained by surface enhanced Raman scattering (SERS) (Vo-Dinh *et al* 1989) due to the presence of silver (confirmed by EDX and XRD) in the sample. As a result of the electron transfer between Ag and ZnO, a strong local electromagnetic field is generated at the interface. The local field thus formed can interact with optical phonons in ZnO nanocrystals which enhance the scattering intensity of active phonons.

Figure 7 represents the room temperature photoluminescence spectrum of ZnO nanorods using an excitation wavelength of 320 nm. The PL spectrum for the ZnO nanorods grown on Ag catalyst shows a strong UV emission peak at ~378·5 nm and a broad defect band centred at 490 nm with a number of shoulder peaks in the visible region. The broad peak can be fitted with Gaussian functions and five Gaussian curves can be extracted from the spectrum (shown in inset of figure 7) with peaks located in the violet region of visible spectrum at 425 nm and 439 nm, peaks in the blue region at 463 nm and 490 nm and a single green peak at 518 nm. The UV emission band is related to a near band-edge (NBE) transition of ZnO. The violet and blue band may appear due to lattice defects related to oxygen and zinc vacancies or interstitials (Hu *et al* 2001). The stronger the intensity of the blue luminescence, the more intrinsic defects (oxygen and zinc vacancies or interstitials) are there. The green band emission is attributed to the radiative recombination of the photo-generated hole with the electron in the singly ionized oxygen vacancy (Vanheusden *et al* 1996). The intensity of the visible emission is mainly dependent on the surface states. Shalish *et al* (2004) reported that below a certain size the luminescence properties are entirely dominated by properties of the surface.

ZnO is a promising sensor material, capable of the detection of flammable, toxic and non-toxic gases. The sensing mechanism is related to the modification of the electrical properties due to the chemical reaction on the oxide surface layer due to the exposure of the sensing gas which causes the change in conduction current. So, gas sensing is a surface phenomena and the sensitivity is dependent on the surface area of the active material. In our work, the surface area of the ZnO films is increased by forming nanostructures where surface to volume ratio is much higher than the bulk crystal. Further efforts to increase the surface area of ZnO were also done by anisotropic etching of patterned Si wafer. The 'V' grooves of etch-patterned wafer provide additional surface area for ZnO growth compared to plain wafer. The nanorods grown on Ag catalyst are sword-like with sharp tips. According to Zhang *et al* (2005) a local charge density and a strong electrostatic field are generated at the tips and the defects of the nanorods which promote the dissociation of some compounds that enhance the sensing action.

Sun *et al* (2006) reported that the ZnO nanorods doped with Ag show enhancement of sensor signal. The presence of silver in ZnO acts as a strong acceptor of electrons from oxide and causes the depletion of electron near the interface. As a result, a space charge region forms at the interface between ZnO and Ag. When the material is

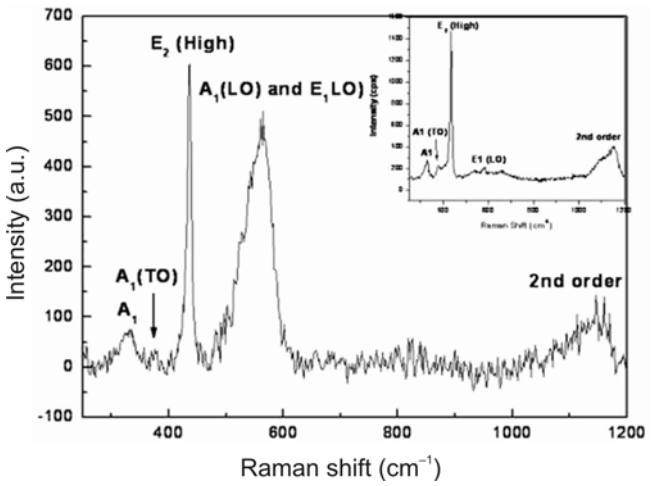

Figure 6. Raman spectrum of ZnO nanorods using 514·5 nm excitation wavelength. Inset shows the Raman spectrum of pure ZnO powder.

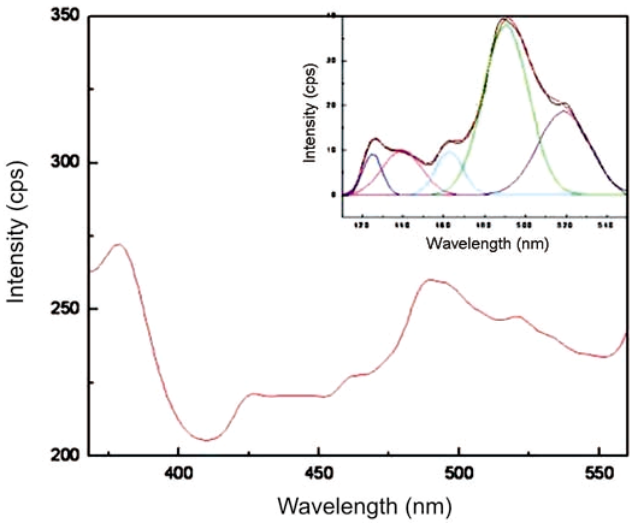

Figure 7. Room temperature PL spectrum of ZnO nanostructures using pulsed Xenon discharge lamp of 320 nm as the excitation source. Inset shows the Gaussian fit of defect emission band.

exposed to the sensing gas, the space charge relaxes by giving electron back to ZnO. This change in space charge height in presence of a sensing gas will change the resistance of the material. In the present work, the EDS spectrum and XRD study confirm the presence of Ag in ZnO film. The surface enhanced Raman spectrum (SERS) also proves the formation of local field at the interface between ZnO and Ag particles. Therefore, the sword-like nanostructures grown on Ag catalyst can be predicted to be a good material for gas sensors.

The intense visible peak in room temperature photoluminescence spectrum indicates that the large surface areas of ZnO are exposed to air and that a large amount of surface states related to oxygen vacancies. Gao *et al* (2005) reported that nanorods having large visible emission band show better gas sensing performance. Therefore, from the above discussion we can predict that the ZnO nanorods grown on annealed silver template over etch-patterned Si wafer is an attractive material for gas sensing applications.

4. Conclusions

Sword-like ZnO nanorods grew successfully on both the oxide mask and in the 'V'-groove of the etch-patterned Si wafer. The surface area of ZnO has been increased by forming nanostructure and growing it over etch-patterned Si wafer. The EDS spectrum and XRD pattern confirm the presence of Ag in the film which acts as growth catalyst for ZnO nanorods. The SERS study proves the presence of local electric field at the metal–ZnO interface and the room temperature photoluminescence spectroscopy indicates that the large amount of surface states related to oxygen vacancies are present. The grown ZnO film can be predicted to be an attractive material for gas sensor. Further studies are being undertaken in this regard.

Acknowledgement

We thank Prof. B Mishra, Geology and Geophysics Department, Indian Institute of Technology, Kharagpur, for giving us the opportunity to do micro-Raman spectroscopy in his laboratory.

References

Ahn S E, Ji H J, Kim K and Kim G T 2007 *Appl. Phys. Lett.* **90** 153106

Alim K A, Fonoberov V A, Shamsa M and Balandin A A 2005 *J. Appl. Phys.* **97** 124313

Choopun S, Hongsith N, Mangkorntong P and Mangkorntong N 2007 *Physica* **E39** 53

Damen T C, Porto S P S and Tell B 1966 *Phys. Rev.* **142** 570

Gao T and Wang T H 2005 *Appl. Phys.* **A80** 1451

Hoefer U, Frank J and Fleischer M 2001 *Sens. Actuators* **B78** 6

Hongsith N, Viriyaworasakul C, Mangkorntong P, Mangkorntong N and Choopun S 2008 *Ceram. Int.* **34** 823

Hsueh T J, Chen Y W, Chang S J, Wang S F, Hsu C L, Lin Y R, Lin T S and Chen I C 2007 *Sens. Actuators* **B125** 498

Hu J Q, Ma X L, Xie Z Y, Wong N B, Lee C S and Lee S T 2001 *Chem. Phys. Lett.* **344** 97

Kim K K, Song J H, Jung H J and Park S J 2000 *J. Appl. Phys.* **87** 3573

Kirkham M, Wang X, Wang Z L and Snyder R L 2007 *Nanotechnol.* **18** 365304

Li C, Hou K, Lei W, Zhang X and Wang B 2007a *Appl. Phys. Lett.* **91** 163502

Li C, Fang G, Guan W and Zhao X 2007b *Mater. Lett.* **61** 3310

Massalski T B (ed.) 1990 *Binary alloy phase diagram* (Materials Park, OH: ASM International), 2nd edn, **Vol. 1**, p 118

Mitra P, Chatterjee A P and Maity H S 1998 *Mater. Lett.* **35** 33

Panda S K, Singh N, Hooda J and Jacob C 2008 *Cryst. Res. Technol.* **43** 751

Panda S K, Singh N, Pal S and Jacob C 2009 *J. Mater. Sci.-Mater. Electron.* **20** 771

Park J Y, Yen Y S, Hong Y S, Oh H, Kim J J and Kim S S 2006 *Composites: Part B* **37** 408

Rao B B 2000 *Mater. Chem. Phys.* **64** 62

Reynolds D C, Look D C and Jogai B 1996 *Solid State Commun.* **99** 873

Rout C S, Hari Krishna S, Vivekchand S R C, Govindaraj A and Rao C N R 2006a *Chem. Phys. Lett.* **418** 586

Rout C S, Raju A R, Govindaraj A and Rao C N R 2006b *Solid State Commun.* **138** 136

Ruiz A M, Sakai G, Cornet A, Shimanoe K, Morante J R and Yamazoe N 2003 *Sens. Actuators* **B93** 509

Sarala Devi G, Bala Subrahmanyam V, Gadkari S C and Gupta S K 2006 *Anal. Chim. Acta* **568** 41

Shalish I, Temkin H and Narayanamurti V 2004 *Phys. Rev.* **B69** 245401

Shishiyanu S T, Shishiyanu T S and Lupan O I 2005 *Sens. Actuators* **B107** 379

Sun Z P, Liu L, Zhang L and Jia D Z 2006 *Nanotechnol.* **17** 2266

Vanheusden K, Warren W L, Seager C H, Tallant D R, Voigt J A and Gnade B E 1996 *J. Appl. Phys.* **79** 7983

Vo-Dinh T, Miller G H, Bello J, Johnson R, Moody R L and Alak A 1989 *Talanta* **36** 227

Wang X, Zhang J, Zhu Z and Zhu J 2007 *Appl. Surf. Sci.* **253** 3168

Xu J, Shun Y, Pan Q and Qin J 2000 *Sens. Actuators* **B66** 161

Zhang Y, Yu K, Jiang D, Zhu Z, Geng H and Luo L 2005 *Appl. Surf. Sci.* **242** 212

Zhang Z Z *et al* 2007 *J. Cryst. Growth* **301–302** 362